Geophysical Research Letters

RESEARCH LETTER
10.1029/2018GL079045

Special Section:
Curiosity at the Bagnold Dunes, Gale crater: Advances in Martian eolian processes

Water Abundance of Dunes in Gale Crater, Mars From Active Neutron Experiments and Implications for Amorphous Phases

T. S. J. Gabriel[1], C. Hardgrove[1], S. Czarnecki[1], E. B. Rampe[2], W. Rapin[3], C. N. Achilles[4], D. Sullivan[1], S. Nowicki[5], L. Thompson[6], M. Litvak[7], I. Mitrofanov[7], and R. T. Downs[8]

[1]School of Earth and Space Exploration, Arizona State University, Tempe, AZ, USA, [2]NASA Johnson Space Center, Houston, TX, USA, [3]California Institute of Technology, Pasadena, CA, USA, [4]NASA Goddard Spaceflight Center, Greenbelt, MD, USA, [5]ISR-1: Space Science and Applications, Los Alamos National Laboratory, Los Alamos, NM, USA, [6]Planetary and Space Science Centre, University of New Brunswick, Fredericton, New Brunswick, Canada, [7]Institute for Space Research, Russian Academy of Sciences, Moscow, Russia, [8]Department of Geosciences, University of Arizona, Tucson, AZ, USA

Abstract We report the water abundance of Bagnold Dune sand in Gale crater, Mars by analyzing active neutron experiments using the Dynamic Albedo of Neutrons instrument. We report a bulk water-equivalent-hydrogen abundance of 0.68 ± 0.15 wt%, which is similar to measurements several kilometers away and from those taken of the dune surface. Thus, the dune is likely dehydrated throughout. Furthermore, we use geochemical constraints, including bulk water content, to develop compositional models of the amorphous fraction for which little information is known. We find the amorphous fraction contains ~26- to 64-wt% basaltic glass and up to ~24-wt% rhyolitic glass, suggesting at least one volcanic source for the dune material. We also find a range of hydrated phases may be present in appreciable abundances, either from the incorporation of eroded aqueously altered sediments or the direct alteration of the dune sand.

Plain Language Summary Dune sands in Gale crater are analagous to the globally distributed sands on Mars; however, their source and history, which is intimately related to their composition, is not well constrained. The minerals that compose the dune sands are determined and constrained from in situ analysis of samples, but much less has been determined for the amorphous (noncrystalline) component. These materials compose a sizable fraction of the dune material (40%) and can provide insight into the history of the dune material, including its interactions with water. We combine the analysis of several instruments onboard the Mars Science Laboratory Curiosity rover to constrain the noncrystalline component of Bagnold Dune sands in Gale crater. Particularly, we find the low water content of the dunes constrains the abundance of several amorphous materials and indicates that at least one, but potentially multiple, volcanic sources contributed to the dune. These results help provide a more holistic compositional description of the Bagnold Dune sands and potentially can be used to help determine the likely source regions in future studies.

Key Points:
- Active neutron experiments show active dunes are the driest material in Gale crater
- Bagnold Dunes are dehydrated throughout; however, the presence of aqueously altered phases could not be ruled out
- Modeling of amorphous compositions shows the origin to be predominantly volcanic, potentially involving multiple or evolving sources

Supporting Information:
- Supporting Information S1

Correspondence to:
T. S. J. Gabriel,
travis.gabriel@asu.edu

Citation:
Gabriel, T. S. J., Hardgrove, C., Czarnecki, S., Rampe, E. B., Rapin, W., Achilles, C. N., et al. (2018). Water abundance of dunes in Gale crater, Mars from active neutron experiments and implications for amorphous phases. *Geophysical Research Letters*, *45*, 12,766–12,775. https://doi.org/10.1029/2018GL079045

Received 1 JUN 2018
Accepted 27 AUG 2018
Accepted article online 4 SEP 2018
Published online 11 DEC 2018

1. Introduction

The Mars Science Laboratory (MSL), Curiosity rover conducted two campaigns to study the composition and morphology of active sand dunes that are found on nearly all sides of the central peak of Gale crater (Mount Sharp). Both campaigns were conducted at the Bagnold Dune Field on the northwest flank of Mount Sharp. Bridges and Ehlmann (2017) provided an overview of the Bagnold phase 1 campaign (sols 1162–1254) and Lapotre and Rampe (2018) provides an overview of the Bagnold phase 2 campaign (sols 1602–1660), the subject of this special issue. The crystalline component of the Bagnold Dunes is primarily mafic; analogous to globally distributed dune sands on Mars (Rampe et al., 2018). X-ray amorphous material constitutes ~40 wt% of Bagnold sand and, by combining results from X-ray spectrometry (for bulk geochemical abundances) and X-ray diffraction (XRD; for mineralogical abundances), the abundance of major rock-forming elements of the amorphous fraction has been constrained (Achilles et al., 2017; Rampe et al., 2018). However, specific amorphous phase abundances have not been constrained using those geochemical estimates. Amorphous

materials can range from relatively unaltered, water-poor materials, for example, glasses, to water-rich materials formed in an aqueous environment; thus, understanding the amorphous fraction of the dune is critical in constraining the alteration history of the sand and its source region, for which there are several candidate locales (Ehlmann et al., 2017). Herein we place constraints on the range of phase abundances in the amorphous fraction and demonstrate that the water content of the material plays an important role. To determine the water content of Bagnold dune sand, we performed in situ active neutron experiments using the Dynamic Albedo of Neutrons (DAN) instrument at the dune. We also compare our results to those of Bagnold phase 1 to examine whether the dunes exhibit compositional variability with depth, lateral distance, and morphology.

2. Background

The Bagnold Dune Field consists primarily of barchan and linear dunes that are spaced ~150–200 m apart and reach heights up to ~10 m (Silvestro et al., 2013). The dune field is active, migrating ~0.4 m per Earth year primarily driven by winds blowing from NE to SW (Bridges et al., 2014; Newman et al., 2017; Silvestro et al., 2013). Near-surface, low-wind-speed, eolian activity is the dominant driver of Bagnold Dune morphology (e.g., Ehlmann et al., 2017; Newman et al., 2017; Sullivan & Kok, 2017). The highly active Namib Dune, studied in Bagnold phase 1, with ripple migration rates of ~1.7 m per Earth year, shows no silt size or finer grains (Ehlmann et al., 2017; Silvestro et al., 2016), likely due to the preferential lofting of smaller grains through eolian activity. Namib Dune has among the lowest water abundances measured along the Curiosity rover's traverse, ~ 0.9±0.3-wt% H_2O as measured by the Sample Analysis at Mars (SAM) instrument evolved gas analysis (EGA) experiments of surficial dune material (Sutter et al., 2017) and 0.8-wt% water equivalent hydrogen (WEH) by active DAN experiments (no reported uncertainty), which are sensitive to ~60-cm depth (Ehlmann et al., 2017). The fact that the dune hydrogen abundance is similarly dehydrated both surficially (Sutter et al., 2017; Stern et al., 2018) and at depth (Ehlmann et al., 2017) and that fine-grained material is considered to be the predominant carrier of hydration in unconsolidated soils (e.g., Ehlmann et al., 2017), suggests that Bagnold dunes lack the fine-grained reservoir throughout (at depth). We note that SAM EGA experiments report H_2S and H_2 as well; however, they are in minimal abundance (~ 10^{-2} wt%).

The Bagnold Dunes are olivine-rich basaltic sand (Achilles et al., 2017; Rampe et al., 2018) with geochemistry similar to the nearby Stimson eolian sandstone formation (Ehlmann et al., 2017; O'Connell-Cooper et al., 2017); however, the Stimson does not contain olivine (Ehlmann et al., 2017). Ehlmann et al. (2017) finds Bagnold sands are geochemically distinct from other unconsolidated materials in Gale crater and from materials measured by the Mars Exploration Rovers. The SAM and DAN instruments indeed found the hydrogen in the active dunes to be depleted with respect to local bedrock (Cousin et al., 2017; Ehlmann et al., 2017; Sutter et al., 2017). Our work herein and recent EGA experiments further corroborate the dehydrated state of the dunes.

Ehlmann et al. (2017) finds there are two reservoirs of water in unconsolidated Martian soils: (1) sand-sized amorphous clasts with bound water and (2) silt-sized amorphous materials primarily with adsorbed and/or loosely bound water. Bagnold dunes in particular lack the dust/silt component, which indicates that the sand-sized amorphous clasts are the dominant volatile reservoir in Bagnold sand. In fact, Ehlmann et al. (2017) reports over 90% of the water in the *Gobabeb* sample, as part of SAM EGA experiments in the Bagnold phase 1 campaign (Sutter et al., 2017), was not adsorbed but was from hydroxylated phases or fluid inclusions.

The amorphous fraction of Bagnold Dunes is 40±15 wt% (Achilles et al., 2017; Rampe et al., 2018), yet its water content is markedly low compared to regions of high amorphous content observed along the traverse such as the silica-rich regions in the Murray and Stimson formations. The *Lubango* target, an opal-rich fracture halo in the Stimson formation, for example, features an amorphous fraction of ~73% and a corresponding water content of 4.0 ± 1.2 WEH (Rapin et al., 2018). This suggests a markedly different inventory and/or hydration state of amorphous phases in active sands. Since amorphous materials can range from water-poor glasses to water-rich products of aqueous alteration, we compute the range of possible phases present in Bagnold Dune sands to complement our understanding of the material as provided by mineralogy. The presence or absence of certain amorphous phases can also be used to help identify the source region of active dune sands in Gale crater.

2.1. Amorphous Material

Amorphous phases lack long-range crystallographic structure, so they do not produce a diagnostic set of sharp peaks in powder XRD patterns, unlike minerals. X-ray amorphous phases produce broad *humps* that can

vary in breadth, position, and number according to chemical composition and the presence of short-range crystallographic ordering. Bish et al. (2013) suggested basaltic glass and allophane were appropriate matches to the amorphous hump found in inactive dune sand at the *Rocknest* target. However, libraries of available X-ray amorphous phases to compare to Chemistry and Mineralogy (CheMin) data are not comprehensive. Ongoing work to build spectral libraries (Achilles et al., 2018) will broaden the catalogue of materials to be modeled in the future. Despite the current limitations in fitting the amorphous XRD hump, geochemical constraints of amorphous materials can be computed by subtracting the mineralogic contribution determined by CheMin XRD from bulk-rock geochemical abundances provided by Alpha Particle X-ray Spectroscopy (APXS) analysis. Using this method, Achilles et al. (2017) and Blake et al. (2013) identified candidate amorphous phases in the *Rocknest* (static dune sample) and *Gobabeb* targets respectively. However, a detailed assessment of the abundances of X-ray amorphous phases in Gale crater sands has not yet been performed until this study.

3. Methodology

We constrain the amorphous composition of Bagnold Dunes by combining two distinct methodologies: (1) active DAN analysis to determine the water content of the bulk subsurface dune material and (2) amorphous phase analysis using a Monte Carlo method to determine the range of amorphous compositions that satisfy the geochemical constraints derived from APXS, CheMin, and DAN. First, we analyze neutron experiments at Ogunquit Beach (see map, Figure S1, in the supporting information) to determine the bulk water content of the dune by fitting modeled spectra to measured spectra using a Markov chain Monte Carlo (MCMC) method. Since hydrous phases in Bagnold Dune sands are hosted predominantly in the amorphous fraction, we translate the bulk water content into that of the amorphous fraction. Finally, we randomly generate mixtures of 11 candidate amorphous phases and report those that satisfy all geochemical constraints on the amorphous fraction, including the DAN-derived bulk water content.

3.1. DAN Measurements

DAN is located at the aft of the Curiosity rover and consists of a pulse neutron generator and two He^3 detectors. In *passive* mode, DAN detects neutrons produced in the Mars surface by cosmic ray bombardment, at energies of 0.001 eV to 1 keV and 0.4 eV to 1 keV in the two He^3 detectors, respectively. In *active* mode, the pulse neutron generator produces 14.1-MeV neutrons via the $^2D + {}^3T \rightarrow n\,(14.1MeV) + {}^4He\,(3.5MeV)$ reaction, for a pulse duration of 1–2 μs. The detectors then measure the moderated neutron flux returning from the subsurface for a 0.1-s window after the pulse, divided into 64 lognormal time bins; the process is repeated for ~12,000 pulses in a standard measurement, each result is coadded to produce a smooth neutron response profile. A more in-depth description of the instrument is provided by Mitrofanov et al. (2012) and Litvak et al. (2008). The shapes of die-away curves depend on the abundance of subsurface elemental hydrogen and neutron absorbers (primarily Cl and Fe [e.g. Hardgrove et al., 2011; Sears, 1992]), the distribution of these elements in the DAN field of view (Mitrofanov et al., 2014), and subsurface bulk density (Mitrofanov et al., 2016). An active DAN surface footprint is ~2 m in diameter and extends to a depth of ~60 cm (Sanin et al., 2015). Thus, DAN complements APXS and the Chemistry and Camera (ChemCam) instrument, which are sensitive to depths of a few micrometers.

Active DAN experiments were performed at Mount Desert Island, a dune in the Bagnold field that overlies bedrock of the Sutton Island member of the Murray formation. The rover was backed over the dune on sol 1659 and two ~12,000 pulse measurements were performed with the instrument surface footprint encompassed completely by dune sand. The water content of the underlying bedrock, which is also in the DAN field of view, was unknown. We determined the water content of the bedrock using coadded data from experiments on sols 1669 and 1671 over a nearby Murray bedrock exposure (see Figure S2).

3.1.1. DAN Modeling and Input Parameters

DAN experiments are compared to the results of neutron transport models using the Monte Carlo N-Particle 6 transport code (MCNP6) developed by Los Alamos National Laboratory (McKinney et al., 2006; Pelowitz, 2008). We used an updated input file template, developed by Jun et al. (2013), that implements major rover components and the DAN instrument; the file was tested against preflight, calibration spectra generated at the Jet Propulsion Laboratory. In contrast, the methods of Sanin et al. (2015) do not include rover components but instead only model an array (ring) of detectors above the Martian surface, and corrections are applied to account for neutron scattering by the rover. The model employed herein is more computationally expensive since neutron-rover interactions are modeled explicitly and only one set of DAN detectors are modeled

(reducing the speed at which the simulation reaches convergence); however, this methodology does not require correction factors.

We modeled the martian subsurface as two layers: a lower-density (1.6 g/cm^3) dune overlying higher-density (1.8 g/cm^3) bedrock. We used measured abundances for the major rock-forming elements of both layers; the lower layer composition sourced from the Sebina bedrock drill target, representative of the Sutton Island member, and the upper layer composition from the Gobabeb target (O'Connell-Cooper et al., 2017; see Table S1). Oxide abundances were converted to elemental abundances, and then to isotopes using terrestrial abundances (Berglund & Wieser 2011), as required by MCNP6. Implicit in this modeling setup is the assumption that the water content of both the bedrock and Bagnold Dune sand is homogeneously distributed and that both are well represented by homogeneously distributed Sebina- and Gobabeb-like geochemistries. Our data-to-model comparison routine, which depends on uncertainty estimation using the MCMC method (Foreman-Mackey et al., 2013) is described further in the supporting information.

3.2. Amorphous Phase Modeling

Specific phases used in modeling the amorphous composition were selected based on FULLPAT analysis of amorphous materials in CheMin data from Ogunquit Beach (Rampe et al., 2018), the geochemistry of the X-ray amorphous component calculated from CheMin and APXS results (Rampe et al., 2018), and X-ray amorphous materials that are common in volcanic terrains on Earth. Basaltic glass, rhyolitic glasses, and ferrihydrite were selected because FULLPAT models of CheMin data from Ogunquit Beach suggest their presence in the sample. Furthermore, volcanic glasses are commonly found in subaerial volcanic rocks, and ferrihydrite is a common incipient weathering product of basalt. We used a Gusev basaltic glass composition (Filiberto et al., 2008) and a rhyolitic glass composition from a glass-bearing inclusion in the Chassigny meteorite (Varela et al., 2000). We assumed a purely Fe-bearing ferrihydrite composition (e.g., no Si substitution or adsorbed ionic complexes). Opal-A was selected because it is a common weathering product in volcanic terrains (e.g., Black & Hynek, 2018; Ehlmann et al., 2012) and was identified on Mars from orbit and in situ within samples from Gale crater (Morris et al., 2016; Rampe et al., 2017; Yen et al., 2017) and Gusev crater (e.g., Ruff et al., 2011; Squyres et al., 2008). We assumed a purely Si-bearing opal-A. Hisingerite and allophane were selected (e.g., Burns, 1986; Rampe et al., 2012); they are common incipient weathering products in volcanic terrains, where hisingerite generally forms in mafic volcanic rocks (Whelan & Goldich, 1961) and allophane forms in glassy deposits (e.g., Wada, 1990). To account for the phosphorus in the amorphous component, amorphous Ca phosphate was selected because of the observation of apatite in CheMin data from mudstone samples from the Murray formation (Rampe et al., 2017) and the precipitation of a Ca phosphate phase in acid-sulfate alteration experiments to mimic the phosphate-rich Martian soil Paso Robles (Hausrath et al., 2013). We selected Fe and Mg sulfates because SAM SO_2 release data indicate their presence in Ogunquit Beach (Stern et al., 2018). We assumed that ferric, rather than ferrous, sulfate is present because of the observation of the crystalline ferric sulfate jarosite in some samples from the Murray formation (Rampe et al., 2017). We selected K and Na sulfate to account for K_2O and Na_2O in the amorphous component. We note that phosphate and sulfate can be chemisorbed onto nanophase weathering products (e.g., Rampe et al., 2016), but we assumed they were present as discrete phases.

3.2.1. Water Content of Amorphous Phases

Water contents for each phase were determined from thermogravimetric (TG) analyses under SAM-like instrument conditions (e.g., carrier gas, pressure, temperature range, and ramp rate) of synthetic amorphous phases or from values reported in the literature. Water contents for ferrihydrite, allophane, and hisingerite were 4, 6.5, and 2.6 wt%, respectively, as measured by TG of synthetic phases (Rampe et al., 2016); hisingerite data are from follow-on experiments from Rampe et al. (2016). SAM data from Ogunquit Beach and Gobabeb suggest Bagnold sands are nearly devoid of adsorbed water; as such, we used H_2O released from 300 to 850 ° C for the water contents for ferrihydrite, allophane, and hisingerite to exclude adsorbed water from our calculations (Sutter et al., 2017). We assumed 0.1-wt% H_2O in both the basaltic and rhyolitic glasses since the parent magma of martian meteorites have <0.3-wt% H_2O (Filiberto & Treiman, 2009). For opal-A, different water contents may be considered as it is known to vary significantly among opals. At Gale crater, opal was identified within silica-rich light-toned alteration halos and with an average opal water content of 6.3 wt% determined from the hydrogen signal in the ChemCam instrument (Rapin, Meslin, et al., 2017; Rapin et al., 2018). However, the SAM instrument yielded a water content of 0.9 ± 0.3 wt% H_2O at the *Greenhorn* alteration halo (Rapin et al., 2018). This difference is interpreted as an effect of sample grinding and preheating, which sig-

nificantly decreases the dehydration temperature of opal (Thomas et al., 2007). Therefore, water content of opal in Bagnold dunes, being a loose powder transported and exposed to the atmosphere, is likely closer the SAM result; thus, we used 2.0-wt% H_2O for the opal-A water content, computed from the bulk SAM EGA value as similarly performed in Rapin et al. (2018). We assumed 22-wt% H_2O in amorphous Mg sulfate based on TG measurements of amorphous Mg sulfate synthesized to investigate their fate on Mars (Vaniman et al., 2004). We assumed 21.26-wt% H_2O in amorphous ferric sulfate based on TG measurements of synthetic amorphous ferric sulfate prepared by vacuum dehydration (Sklute et al., 2015), but the samples were not allowed a similar amount of time to equilibrate in Martian conditions as were those of Vaniman et al. (2004). We assumed K sulfate, Na sulfate, and Ca phosphate were anhydrous because, although water can adsorb to the surfaces of crystalline K sulfate and Na sulfate (e.g., Balić-Žunić et al., 2016; Herrero et al., 2015) and synthetic amorphous Ca phosphate (e.g., Li et al., 2007), SAM data suggest active sands in Gale crater generally lack adsorbed water (Stern et al., 2018). The geochemical abundances of the modeled amorphous phases are summarized in Table S2.

4. Results

4.1. Bulk Dune Hydration Analysis

Our analysis of the underlying Murray bedrock indicates a bulk water content of 4.2 ± 0.51 WEH (1σ; see Figure S4). This relatively high water content is likely due to the presence of clays (~19 wt%), jarosite (~0.9 wt%), and amorphous material (~51 wt%) that were seen in the Sebina drill sample of the Murray (Bristow et al., 2018). Using this result to inform our two-layer models that feature the dune sand and underlying bedrock, we find a bulk water content of 0.68 ± 0.15 WEH (1σ) for the dune sand at Ogunquit Beach (see Figure 1), which agrees well with SAM results at the same location (0.8 ± 0.3-wt% H_2O). These results also agree with active DAN results during Bagnold phase 1 that found 0.8 WEH (no reported uncertainty; Ehlmann et al., 2017) and SAM results at the same location (0.9 ± 0.3-wt% H_2O). The low water content of the dune compared to other unconsolidated sediments in Gale crater is also consistent with the hydrogen signal measured by ChemCam laser-induced breakdown spectroscopy experiments (see Figure S5; Rapin, Bousquet, et al., 2017; Rapin et al., 2018). It shows qualitatively that active dunes measured during Bagnold phases 1 and 2 have the same hydration signature, lower than fine-grained soils encountered along the traverse (Cousin et al., 2014, 2017; Forni et al., 2013).

4.2. Amorphous Component Analysis

To constrain the range of amorphous phases in the Bagnold Dunes, we perform a Monte Carlo procedure to randomly generate mixtures of 11 candidate amorphous phases. The geochemical abundances of each mixture are compared to measured abundances from CheMin XRD and APXS analysis determined for the amorphous fraction (O'Connell-Cooper et al., 2017; Rampe et al., 2018; see Table S3 for the geochemical constraints). Figure 2 shows the range of models that fit all geochemical constraints (colored points), compared to those that do not fit the water content constraint (gray points). We find that the amorphous fraction contains 19.6- to 66.9-wt% basaltic glass, and up to 29.5 wt% rhyolitic glass, 35.7 wt% opal, 15.5 wt% allophane, 15.7 wt% hisingerite, and 11.5 wt% ferrihydrite (see Figure 2).

We find the good-fit models constrained by geochemical abundances provided from APXS and CheMin experiments span a range ~1.0- to 5.0-wt% H_2O. A smaller range of allowable water abundance is provided by the active DAN results herein. We first assume water is primarily in the amorphous fraction since hydrated crystalline minerals were below CheMin detection limits at Bagnold phase 1 (Achilles et al., 2017). The Ogunquit Beach sample is similarly devoid of hydrated crystalline phases; a ~7-wt% phyllosilicate feature in the XRD pattern is likely due to contamination from a previous sample (Rampe et al., 2018). The oxide abundance constraints for the amorphous fraction used herein have been renormalized to account for the contamination (Rampe et al., 2018). To translate our water abundance of the bulk into that of the amorphous material, we require an estimate of the amorphous fraction. The minimum abundance of X-ray amorphous material is 33 wt% at Ogunquit Beach (Rampe et al., 2018), as constrained from a combination of APXS and CheMin analysis. The maximum abundance is constrained by FULLPAT analysis of the X-ray amorphous hump and Rampe et al. (2018) finds a best fit value of 40 ± 15 wt%. Thus, at Ogunquit Beach, we assume that the amorphous fraction ranges from 33 wt% (constrained by APXS and CheMin) to 55 wt% (constrained by CheMin FULLPAT analysis), with a mean of 44 wt%. This allows the water abundance measured in the *bulk* sand to be translated to the abundance of the amorphous fraction, $(0.68 \pm 0.15 \text{ WEH})/(44 \pm 11 \text{ wt\% } (3\sigma)) = 1.55 \pm 0.36$ WEH (1σ). We note that decreasing the bulk density assumption of the dune sand in our MCNP6 models by 0.2 g/cm^3 produces best fit water estimates that are ~0.15 WEH lower.

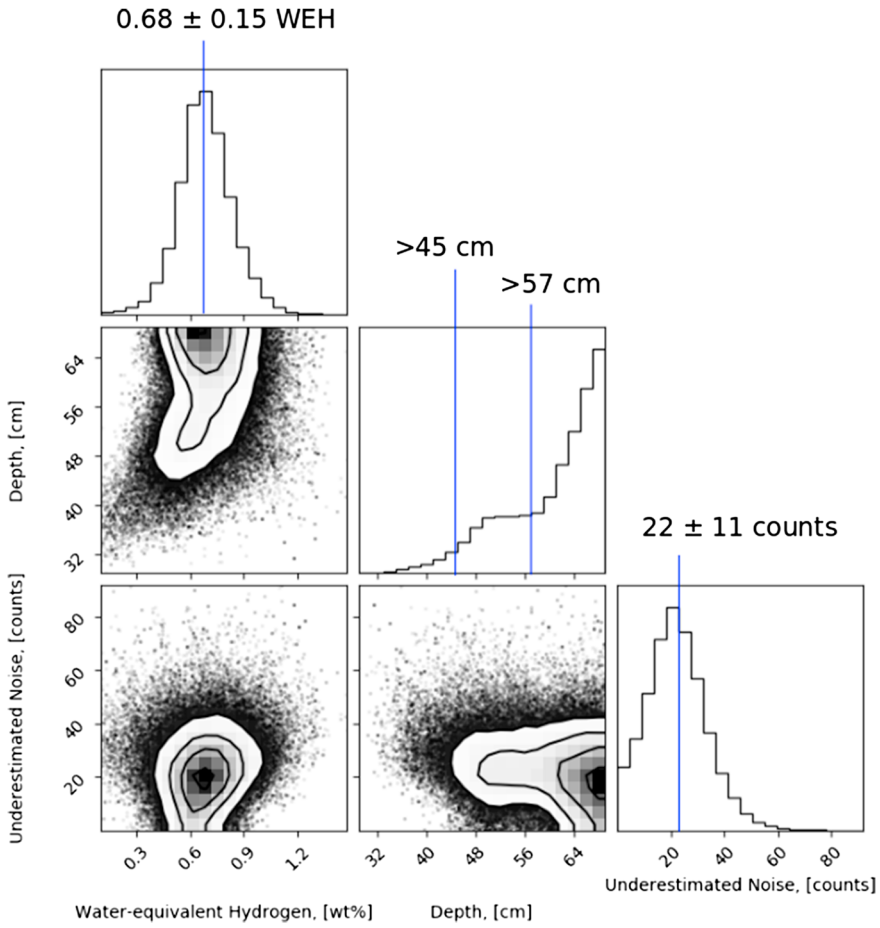

Figure 1. Shown are the a posteriori distributions of the fitted parameters determined from analysis of the active Dynamic Albedo of Neutrons experiment at Bagnold phase 2. The marginalized distributions are projected as histograms along the diagonal. The mean and standard deviation of the water content of the top layer (dune) is 0.68 ± 0.15 WEH, and the underestimated uncertainty is $f = 22 \pm 11$ counts, with a correlation coefficient of 0.14 between the two parameters. Depths ≥57 cm encompass 68% of the likelihood (1σ), and depths ≥45 cm encompass 95% (2σ). WEH = wt% water equivalent hydrogen.

5. Discussion

Active neutron experiments at Bagnold phase 1 (Ehlmann et al., 2017) indicated that Bagnold Dunes are depleted in water (~0.8 WEH) compared to all materials examined by active neutron experiments in Gale crater to date (Litvak et al., 2016; Mitrofanov et al., 2014); however, Sutter et al. (2017) reported a water content of 1.1 ± 0.5 WEH. The upper end of this range is similar to the abundance in bedrock targets reported therein and in Mitrofanov et al. (2014). Our results at Bagnold phase 2 confirm that Bagnold sands indeed contain depleted levels of water (0.68 ± 0.15 WEH). This is consistent with the latest SAM EGA results at Bagnold phase 2 (0.8 ± 0.3 WEH) and with refinements of the Bagnold phase 1 measurements (0.9 ± 0.3 WEH; Stern et al., 2018). ChemCam laser-induced breakdown spectroscopy hydrogen peaks are also systematically lower for active dune sands than those of inactive bedforms with a greater fraction of fine-grained components. Since the sensing area of active DAN experiments reaches to depths of ~60 cm (Sanin et al., 2015) and SAM EGA experiments are sensitive to scooped samples from the dune surface, our results indicate the water distribution, or equivalently, the distribution of hydrated amorphous reservoirs, are likely homogeneous with depth in the dune body. This finding suggests eolian activity efficiently mixes grains in the active dunes over time, potentially through the entirety of the dune.

Since Bagnold Dune sands lack appreciable hydrated minerals (Achilles et al., 2017; Rampe et al., 2018), the amorphous fraction (44 ± 11 wt%) is the primary source of the measured water content. Water in Bagnold sands is suggested to be sourced from a coarse-grained ($\gtrapprox$150 μm), silica-rich reservoir with partially

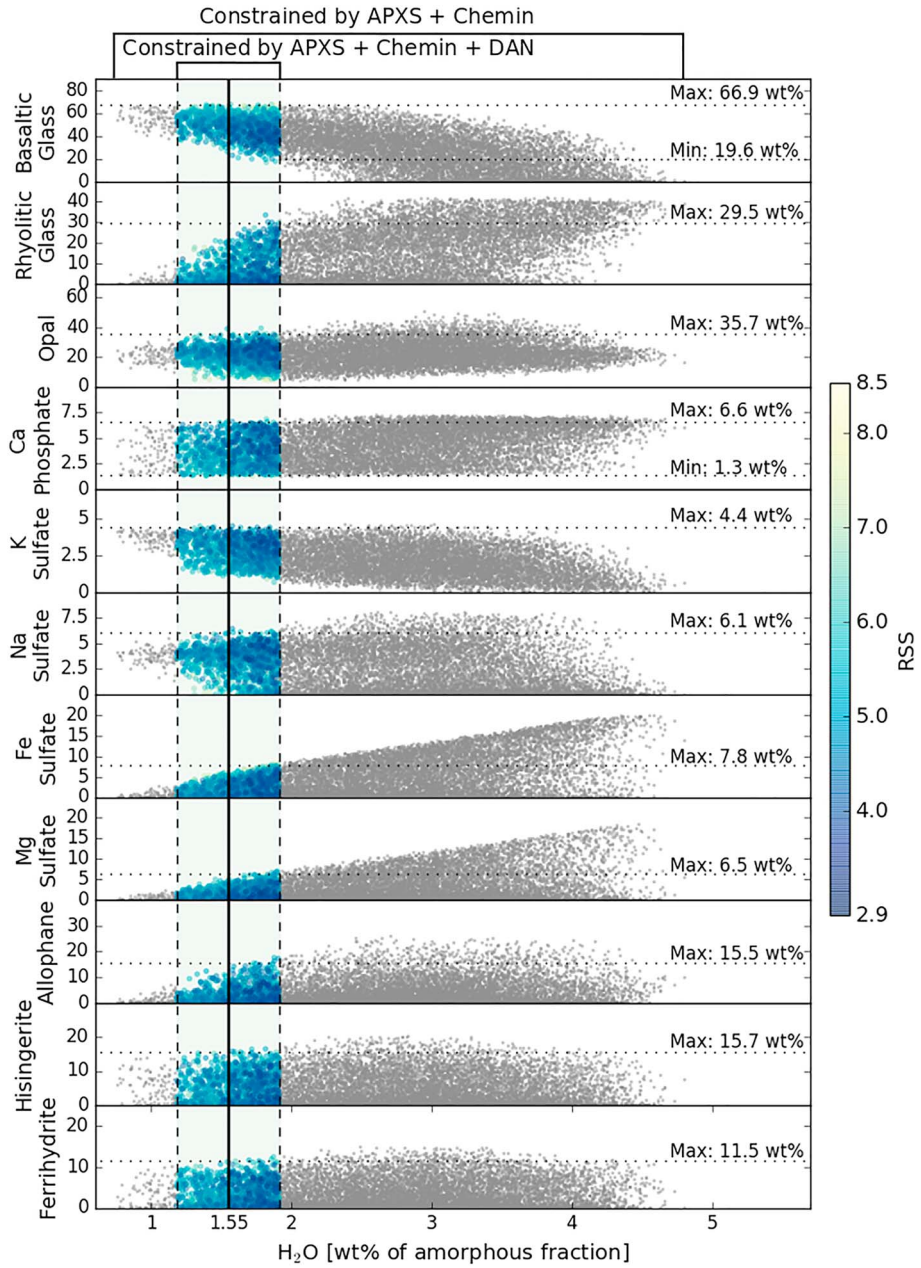

Figure 2. Shown are 10,000 randomly generated models that satisfy oxide constraints on the amorphous fraction of Bagnold sands. Each model is represented by a single point in each panel. The y axis is the abundance of a particular phase in weight percent of the amorphous fraction, and the x axis is the water content of the amorphous fraction. The vertical dashed lines represent the allowed range of water content of the amorphous fraction, as measured by DAN. Colors represent the root of the sum of squares of the deviations of the models from the target or *RSS*. Darker colors are models with lower deviations from oxide constraints. The reported minima and maxima are 3σ estimates computed using a bootstrap resampling (10^5 samples). APXS = Alpha Particle X-ray Spectroscopy; CheMin = Chemistry and Mineralogy; DAN = Dynamic Albedo of Neutrons.

hydroxylated products of alteration, bound water/OH in glass, or both, in contrast to the source for inactive dunes: a fine-grained ($\lessapprox$150 μm), silica-poor reservoir with mostly loosely bound and adsorbed water (Ehlmann et al., 2017). Indeed, SAM EGA experiments of Bagnold Dune sand find that the temperature of peak water release is at >300 ° C (Stern et al., 2018; Sutter et al., 2017), which indicates an absence of significant amounts of adsorbed water. Thus, the water abundance derived for the amorphous content herein, 1.55±0.36 WEH is an in situ measurement of the water content in the coarse-grained reservoir.

Using constraints from the DAN analysis, in addition to constraints from CheMin (Rampe et al., 2018) and APXS (O'Connell-Cooper et al., 2018), we find that basaltic glass composes at least 19.6 wt% of the amorphous fraction (~8.6 wt% of the bulk), necessitating a volcanic source for Bagnold Dune sand. Good-fit models (Figure 2) also allow for significant abundances of rhyolitic glass, opal, and hisingerite; however, these phases are the predominant carriers of silica, which leads to model solutions consistent with anticorrelated abundances of these phases. For example, as shown in Figure S6, models with high abundances of opal have correspondingly low abundances of rhyolitic glass (anticorrelation). However, opal is positively correlated with ferrihydrite to compensate for the losses in Fe in opal-rich geochemistries.

Our result is consistent with Achilles et al. (2017) that found the X-ray amorphous hump pattern can be modeled with a mixture of basaltic and rhyolitic glass; however, it is still likely that hydrated phases are present to account for the measured water content, motivating the development of additional X-ray spectral libraries for amorphous materials. We find that each of the modeled sulfates are limited to abundances of at most ~4 - 8 wt% of the amorphous fraction, but their presence in good-fit models is consistent with SAM EGA experiments of the Ogunquit Beach sample, which indicate the existence of these phases from high SO_2 release temperatures (500–800 °C; Stern et al., 2018).

We predict the source region of Bagnold Dunes should contain water contents no less than 0.68 ± 0.15-wt% H_2O since Bagnold sands have had ample opportunity to equilibrate with the Martian low vapor pressure atmosphere and thus are likely dehydrated with respect to their source. The presence of basaltic glass indicates that Bagnold sands include contributions from at least one volcanic source for the dune sand, but the presence of rhyolitic glass in good-fit models also indicates that Bagnold sands potentially include contributions from a silicic volcanic source. A single source for both volcanic glasses is also possible; however, this would require eruptions of an evolving magmatic body. Products of aqueous alteration, namely, opal, allophane, hisingerite, and ferrihydrite are also possible in appreciable abundances in Bagnold dunes. It is thus possible that aqueously altered sediments contributed to the Bagnold Dune sand or that the sand was directly altered.

6. Conclusion

We find that hydrated phases in the Bagnold Dune Field are likely homogeneously distributed at depth and laterally, across kilometer scales. Specifically, we find the dune sand to have a bulk water content of 0.68 ± 0.15 WEH near Ogunquit Beach, which is consistent with similar active neutron measurements by the DAN instrument near *Gobabeb* (~0.8 WEH; Ehlmann et al., 2017), located several kilometers north in the same dune field. SAM EGA experiments show that sand scooped from the dune surface has 0.8 ± 0.3 WEH at *Ogunquit Beach* and 0.9 ± 0.3 WEH at *Gobabeb* (Stern et al., 2018), which agrees with our results. Considering that DAN is sensitive to the top ~60 cm (Sanin et al., 2015) and that SAM is sensitive to the shallow, scooped dune material, we conclude that the distribution of water and the associated coarse-grained amorphous reservoir are homogeneous throughout the Bagnold Dunes.

Since hydrated crystalline phases were not observed above CheMin detection limits and >90% of the water is bound (nonadsorbed) water (Achilles et al., 2018; Ehlmann et al., 2017; Rampe et al., 2018), the Bagnold Dune sands provide the unique opportunity to directly measure the hydration state of the bound water in the amorphous fraction. Using the DAN-derived water content, in addition to APXS and CheMin analysis, we constrained the maximum and minimum abundances of 11 candidate amorphous phases for Bagnold Dune sands. Specifically, we find that the Bagnold Dunes likely contain 19.6- to 66.9-wt% basaltic glass in the amorphous fraction (~8.6- to 29.4-wt% in the bulk). However, our results do not preclude the the possibility that the Bagnold Dunes contain material sourced from silica-rich volcanic complexes since the composition of rhyolitic glass can be in abundances of 0- to 29.5-wt% in the amorphous fraction (~0- to 13.0-wt% in the bulk). Future work will involve the fitting of these models to the amorphous hump in XRD patterns to further constrain the amorphous material, effectively testing the range of amorphous compositions derived herein. We conclude that the amorphous composition of the Bagnold Dune sand necessitates a complex history that includes one or more volcanic sources. It is also possible that Bagnold Dune sand was directly altered or that aqueously altered bedrock sediment contributed to the dune sand.

Acknowledgments
We acknowledge the Dynamic Albedo of Neutrons instrument team and the broader Mars Science Laboratory team. This work was supported by the Mars Science Laboratory Participating Scientist Program, award number NNN12AA01C, and by the NASA Earth and Space Science Fellowship, award PLANET17F-0107. Computational support was provided in part by the Space Science and Applications group at Los Alamos National Laboratory and by the Research Computing center at Arizona State University. The authors thank Michael Line at Arizona State University for providing insight into statistical methods used herein and the authors thank Jack Lightholder at Jet Propulsion Laboratory for his early contributions to the project. All data from this work are publicly accessible on the Planetary Data System, www.pds.nasa.gov.

References

Achilles, C. N., Downs, G. W., Downs, R. T., Morris, R. V., Rampe, E. B., Ming, D. W., et al. (2018). Amorphous phase characterization through X-ray diffraction profile modeling: Implications for amorphous phases in Gale Crater rocks and soils. In *49th Lunar and Planetary Science Conference* (pp. 2661). Houston, TX.

Achilles, C. N., Downs, R. T., Ming, D. W., Rampe, E. B., Morris, R. V., Treiman, A. H., et al. (2017). Mineralogy of an active eolian sediment from the Namib dune, Gale crater, Mars. *Journal of Geophysical Research: Planets*, *122*, 2344–2361. https://doi.org/10.1002/2017JE005262

Balić-Žunić, T., Birkedal, R., Katerinopoulou, A., & Comodi, P. (2016). Dehydration of blödite, $Na_2Mg(SO_4)_2(H_2O)_4$, and leonite, $K_2Mg(SO_4)_2(H_2O)_4$. *European Journal of Mineralogy*, *28*(1), 33–42. https://doi.org/10.1127/ejm/2015/0027-2487

Bish, D. L., Blake, D. F., Vaniman, D. T., Chipera, S. J., Morris, R. V., Ming, D. W., et al. (2013). X-ray diffraction results from Mars Science Laboratory: Mineralogy of Rocknest at Gale Crater. *Science*, *341*(6153). https://doi.org/10.1126/science.1238932

Black, S. R., & Hynek, B. M. (2018). Characterization of terrestrial hydrothermal alteration products with Mars analog instrumentation: Implications for current and future rover investigations. *Icarus*, *307*, 235–259. https://doi.org/10.1016/j.icarus.2017.10.032

Blake, D. F., Morris, R. V., Kocurek, G., Morrison, S. M., Downs, R. T., Bish, D., et al. (2013). Curiosity at Gale Crater, Mars: Characterization and analysis of the Rocknest sand shadow. *Science*, *341*(6153). https://doi.org/10.1126/science.1239505

Bridges, N. T., Calef, F. J., Hallet, B., Herkenhoff, K. E., Lanza, N. L., Le Mouélic, S., et al. (2014). The rock abrasion record at Gale Crater: Mars Science Laboratory results from Bradbury Landing to Rocknest. *Journal of Geophysical Research: Planets*, *119*, 1374–1389. https://doi.org/10.1002/2013JE004579

Bridges, N. T., & Ehlmann, B. L. (2017). The Mars Science Laboratory (MSL) Bagnold Dunes campaign, Phase I: Overview and introduction to the special issue. *Journal of Geophysical Research: Planets*, *123*, 3–19. https://doi.org/10.1002/2017JE005401

Bristow, T. F., Rampe, E. B., Achilles, C. N., Blake, D. F., Chipera, S. J., Craig, P., et al. (2018). Clay mineral diversity and abundance in sedimentary rocks of Gale crater, Mars. *Science Advances*, *4*(6), eaar3330. https://doi.org/10.1126/sciadv.aar3330

Burns, R. G. (1986). Terrestrial analogues of the surface rocks of Mars? *Nature*, *320*, 55–56. https://doi.org/10.1038/320055a0

Berglund, M., & Wieser, M. E. (2011). Isotopic compositions of the elements 2009 (IUPAC Technical Report). *Pure and Applied Chemistry*, *83*(2), 397–410. https://doi.org/10.1351/PAC-REP-10-06-02

Cousin, A., Clegg, S. M., Dehouck, E., Fabre, C., Forni, O., Gasnault, O., et al. (2014). ChemCam blind targets: A helpful way of analyzing soils and rocks along the traverse. In *45th Lunar and Planetary Science Conference* (pp. 1278). Houston, TX.

Cousin, A., Dehouck, E., Meslin, P.-Y., Forni, O., Williams, A. J., Stein, N., et al. (2017). Geochemistry of the Bagnold dune field as observed by ChemCam and comparison with other aeolian deposits at Gale Crater. *Journal of Geophysical Research: Planets*, *122*, 2144–2162. https://doi.org/10.1002/2017JE005261

Ehlmann, B. L., Bish, D. L., Ruff, S. W., & Mustard, J. F. (2012). Mineralogy and chemistry of altered Icelandic basalts: Application to clay mineral detection and understanding aqueous environments on Mars. *Journal of Geophysical Research*, *117*, E00J16. https://doi.org/10.1029/2012JE004156

Ehlmann, B. L., Edgett, K. S., Sutter, B., Achilles, C. N., Litvak, M. L., Lapotre, M. G. A., et al. (2017). Chemistry, mineralogy, and grain properties at Namib and High dunes, Bagnold dune field, Gale crater, Mars: A synthesis of Curiosity rover observations. *Journal of Geophysical Research: Planets*, *122*, 2510–2543. https://doi.org/10.1002/2017JE005267

Filiberto, J., & Treiman, A. H. (2009). Martian magmas contained abundant chlorine, but little water. *Geology*, *37*(12), 1087–1090. https://doi.org/10.1130/G30488A.1

Filiberto, J., Treiman, A. H., & Le, L. (2008). Crystallization experiments on a Gusev Adirondack basalt composition. *Meteoritics and Planetary Science*, *43*(7), 1137–1146. https://doi.org/10.1111/j.1945-5100.2008.tb01118.x

Foreman-Mackey, D., Hogg, D. W., Lang, D., & Goodman, J. (2013). emcee: The MCMC Hammer. *The Astronomical Society of the Pacific*, *125*(925), 306–312. https://doi.org/10.1086/670067

Forni, O., Maurice, S., Gasnault, O., Wiens, R. C., Cousin, A., Clegg, S. M., et al. (2013). Independent component analysis classification of laser induced breakdown spectroscopy spectra. *Spectrochimica Acta Part B: Atomic Spectroscopy*, *86*, 31–41. https://doi.org/10.1016/j.sab.2013.05.003

Hardgrove, C., Moersch, J., & Drake, D. (2011). Effects of geochemical composition on neutron die-away measurements: Implications for Mars Science Laboratory's Dynamic Albedo of Neutrons experiment. *Nuclear Instruments and Methods in Physics Research, Section A: Accelerators, Spectrometers, Detectors and Associated Equipment*, *659*(1), 442–455. https://doi.org/10.1016/j.nima.2011.08.058

Hausrath, E. M., Golden, D. C., Morris, R. V., Agresti, D. G., & Ming, D. W. (2013). Acid sulfate alteration of fluorapatite, basaltic glass and olivine by hydrothermal vapors and fluids: Implications for fumarolic activity and secondary phosphate phases in sulfate-rich Paso Robles soil at Gusev Crater, Mars. *Journal of Geophysical Research: Planets*, *118*, 1–13. https://doi.org/10.1029/2012JE004246

Herrero, M. J., Escavy, J. I., & Schreiber, B. C. (2015). Thenardite after mirabilite deposits as a cool climate indicator in the geological record: Lower Miocene of central Spain. *Climate of the Past*, *11*(1), 1–13. https://doi.org/10.5194/cp-11-1-2015

Jun, I., Mitrofanov, I., Litvak, M. L., Sanin, A. B., Kim, W., Behar, A., et al. (2013). Neutron background environment measured by the Mars Science Laboratory's Dynamic Albedo of Neutrons instrument during the first 100 sols. *Journal of Geophysical Research: Planets*, *118*, 2400–2412. https://doi.org/10.1002/2013JE004510

Lapotre, M. G. A., & Rampe, E. B. (2018). Curiosity's investigation of the Bagnold Dunes, Gale crater: Overview of the two-phase scientific campaign and introduction to the special collection. *Journal of Geophysical Research: Planets*, *123*. https://doi.org/10.1029/2018GL079032

Li, Y., Wiliana, T., & Tam, K. C. (2007). Synthesis of amorphous calcium phosphate using various types of cyclodextrins. *Materials Research Bulletin*, *42*(5), 820–827. https://doi.org/10.1016/j.materresbull.2006.08.027

Litvak, M. L., Mitrofanov, I. G., Barmakov, Y. N., Behar, A., Bitulev, A., Bobrovnitsky, Y., et al. (2008). The Dynamic Albedo of Neutrons (DAN) Experiment for NASA's 2009 Mars Science Laboratory. *Astrobiology*, *8*(3), 605–612. https://doi.org/10.1089/ast.2007.0157

Litvak, M. L., Mitrofanov, I. G., Hardgrove, C., Stack, K. M., Sanin, A. B., Lisov, D., et al. (2016). Hydrogen and chlorine abundances in the Kimberley formation of Gale crater measured by the DAN instrument on board the Mars Science Laboratory Curiosity rover. *Journal of Geophysical Research: Planets*, *121*, 836–845. https://doi.org/10.1002/2015JE004960

McKinney, G. W., Durkee, J. W., Hendricks, J. S., James, M. R., Pelowitz, D. B., Waters, L. S., & Gallmeier, F. X. (2006). *MCNPX overview, Proceedings of the 2006 HSSW, FNAL*. Los Alamos, NM: Los Alamos National Laboratory.

Mitrofanov, I. G., Kozyrev, A. S., Lisov, D. I., Vostrukhin, A. A., Golovin, D. V., Litvak, M. L., et al. (2016). Active neutron sensing of the Martian surface with the DAN experiment onboard the NASA "Curiosity" Mars rover: Two types of soil with different water content in the Gale crater. *Astronomy Letters*, *42*(4), 251–259. https://doi.org/10.1134/S1063773716040058

Mitrofanov, I. G., Litvak, M. L., Sanin, A. B., Starr, R. D., Lisov, D. I., Kuzmin, R. O., et al. (2014). Water and chlorine content in the Martian soil along the first 1900 m of the Curiosity rover traverse as estimated by the DAN instrument. *Journal of Geophysical Research: Planets*, *119*, 1579–1596. https://doi.org/10.1002/2013JE004553

Mitrofanov, I. G., Litvak, M. L., Varenikov, A. B., Barmakov, Y. N., Behar, A., Bobrovnitsky, Y. I., et al. (2012). Dynamic Albedo of Neutrons (DAN) experiment onboard NASA's Mars Science Laboratory. *Space Science Reviews*, *170*(1–4), 559–582. https://doi.org/10.1007/s11214-012-9924-y

Morris, R. V., Vaniman, D. T., Blake, D. F., Gellert, R., Chipera, S. J., Rampe, E. B., et al. (2016). Silicic volcanism on Mars evidenced by tridymite in high-SiO_2 sedimentary rock at Gale crater. *Proceedings of the National Academy of Sciences of the United States of America*, *113*(26), 7071–7076. https://doi.org/10.1073/pnas.1607098113

Newman, C. E., Gómez-Elvira, J., Marin, M., Navarro, S., Torres, J., Richardson, M. I., et al. (2017). Winds measured by the Rover Environmental Monitoring Station (REMS) during the Mars Science Laboratory (MSL) rover's Bagnold Dunes Campaign and comparison with numerical modeling using MarsWRF. *Icarus*, *291*, 203–231. https://doi.org/10.1016/j.icarus.2016.12.016

O'Connell-Cooper, C. D., Spray, J. G., Thompson, L. M., Gellert, R., Berger, J. A., Boyd, N. I., et al. (2017). APXS-derived chemistry of the Bagnold dune sands: Comparisons with Gale Crater soils and the global Martian average. *Journal of Geophysical Research: Planets*, *122*, 2623–2643. https://doi.org/10.1002/2017JE005268

O'Connell-Cooper, C. D., Thompson, L. M., Spray, J. G., Berger, J. A., VanBommel, S. J., Gellert, R., et al. (2018). Chemical diversity of sands within the linear and barchan dunes of the Bagnold Dunes, Gale Crater, as revealed by APXS onboard Curiosity. *Geophysical Research Letters*, *45*. https://doi.org/10.1029/2018GL079026

Pelowitz, D. B. (2008). *MNCPX user's manual, version 2.6.0*. Los Alamos, NM: Los Alamos National Laboratory.

Rampe, E. B., Lapotre, M. G. A., Bristow, T. F., Arvidson, R. E., Morris, R. V., Achilles, C. N., et al. (2018). Sand mineralogy within the Bagnold dunes, Gale Crater, as observed in situ and from orbit. *Journal of Geophysical Research: Planets*, *123*. https://doi.org/10.1029/2018GL079073

Rampe, E. B., Kraft, M. D., Sharp, T. G., Golden, D. C., Ming, D. W., & Christensen, P. R. (2012). Allophane detection on Mars with Thermal Emission Spectrometer data and implications for regional-scale chemical weathering processes. *Geology*, *40*(11), 995–998. https://doi.org/10.1130/G33215.1

Rampe, E. B., Ming, D. W., Blake, D. F., Bristow, T. F., Chipera, S. J., Grotzinger, J. P., et al. (2017). Mineralogy of an ancient lacustrine mudstone succession from the Murray formation, Gale crater, Mars. *Earth and Planetary Science Letters*, *471*, 172–185. https://doi.org/10.1016/j.epsl.2017.04.021

Rampe, E. B., Morris, R. V., Archer, P. D., Agresti, D. G. Jr, & Ming, D. W. (2016). Recognizing sulfate and phosphate complexes chemisorbed onto nanophase weathering products on Mars using in-situ and remote observations. *American Mineralogist*, *101*(3), 678–689. https://doi.org/10.2138/am-2016-5408CCBYNCND

Rapin, W., Bousquet, B., Lasue, J., Meslin, P.-Y., Lacour, J.-L., Fabre, C., et al. (2017). Roughness effects on the hydrogen signal in laser-induced breakdown spectroscopy. *Spectrochimica Acta Part B: Atomic Spectroscopy*, *137*, 13–22. https://doi.org/10.1016/j.sab.2017.09.003

Rapin, W., Chauviré, B., Gabriel, T. S. J., McAdam, A. C., Ehlmann, B. L., Hardgrove, C., et al. (2018). In situ analysis of opal in Gale crater, Mars. *Journal of Geophysical Research: Planets*, *123*. https://doi.org/10.1029/2017JE005483

Rapin, W., Meslin, P.-Y., Maurice, S., Wiens, R. C., Laporte, D., Chauviré, B., et al. (2017). Quantification of water content by laser induced breakdown spectroscopy on Mars. *Spectrochimica Acta Part B: Atomic Spectroscopy*, *130*, 82–100. https://doi.org/10.1016/j.sab.2017.02.007

Ruff, S. W., Farmer, J. D., Calvin, W. M., Herkenhoff, K. E., Johnson, J. R., Morris, R. V., et al. (2011). Characteristics, distribution, origin, and significance of opaline silica observed by the Spirit rover in Gusev crater, Mars. *Journal of Geophysical Research*, *116*, E00F23. https://doi.org/10.1029/2010JE003767

Sanin, A. B., Mitrofanov, I. G., Litvak, M. L., Lisov, D. I., Starr, R., Boynton, W., et al. (2015). Data processing of the active neutron experiment DAN for a Martian regolith investigation. *Nuclear Instruments and Methods in Physics Research Section A: Accelerators, Spectrometers, Detectors and Associated Equipment*, *789*, 114–127. https://doi.org/10.1016/j.nima.2015.03.085

Sears, V. F. (1992). Neutron scattering lengths and cross sections. *Neutron News*, *3*(3), 26–37. https://doi.org/10.1080/10448639208218770

Silvestro, S., Vaz, D. A., Ewing, R. C., Rossi, A. P., Fenton, L. K., Michaels, T. I., et al. (2013). Pervasive aeolian activity along rover Curiosity's traverse in Gale Crater, Mars. *Geology*, *41*(4), 483–486. https://doi.org/10.1130/G34162.1

Silvestro, S., Vaz, D. A., Yizhaq, H., & Esposito, F. (2016). Dune-like dynamic of Martian Aeolian large ripples. *Geophysical Research Letters*, *43*, 8384–8389. https://doi.org/10.1002/2016GL070014

Sklute, E. C., Jensen, H. B., Rogers, A. D., & Reeder, R. J. (2015). Morphological, structural, and spectral characteristics of amorphous iron sulfates. *Journal of Geophysical Research: Planets*, *120*, 809–830. https://doi.org/10.1002/2014JE004784

Squyres, S. W., Arvidson, R. E., Ruff, S., Gellert, R., Morris, R. V., Ming, D. W., et al. (2008). Detection of silica-rich deposits on Mars. *Science*, *320*(5879), 1063–1067. https://doi.org/10.1126/science.1155429

Stern, J. C., Sutter, B., Archer, P. D., Eigenbrode, J. L., McAdam, A. C., Franz, H. B., et al. (2018). Major volatiles evolved from eolian materials in Gale crater. *Geophysical Research Letters*, *45*. https://doi.org/10.1029/2018GL079059

Sullivan, R., & Kok, J. F. (2017). Aeolian saltation on Mars at low wind speeds. *Journal of Geophysical Research: Planets*, *122*, 2111–2143. https://doi.org/10.1002/2017JE005275

Sutter, B., McAdam, A. C., Mahaffy, P. R., Ming, D. W., Edgett, K. S., Rampe, E. B., et al. (2017). Evolved gas analyses of sedimentary rocks and eolian sediment in Gale Crater, Mars: Results of the Curiosity rover's sample analysis at Mars instrument from Yellowknife Bay to the Namib Dune. *Journal of Geophysical Research: Planets*, *122*, 2574–2609. https://doi.org/10.1002/2016JE005225

Thomas, P. S., Simon, P., Smallwood, A., & Ray, A. S. (2007). Estimation of the diffusion coefficient of water evolved during the non-isothermal dehydration of australian sedimentary opal. *Journal of Thermal Analysis and Calorimetry*, *88*(1), 231–235. https://doi.org/10.1007/s10973-006-8133-x

Vaniman, D. T., Bish, D. L., Chipera, S. J., Fialips, C. I., William Carey, J., & Feldman, W. C. (2004). Magnesium sulphate salts and the history of water on Mars. *Nature*, *431*, 663–665. https://doi.org/10.1038/nature02973

Varela, M. E., Kurat, G., Bonnin-Mosbah, M., Clocchiatti, R., & Massare, D. (2000). Glass-bearing inclusions in olivine of the Chassigny achondrite: Heterogeneous trapping at sub-igneous temperatures. *Meteoritics and Planetary Science*, *35*(1), 39–52. https://doi.org/10.1111/j.1945-5100.2000.tb01972.x

Wada, K. (1990). Minerals in soil environments. *Soil Science*, *150*(2), 1051–1087.

Whelan, J. A., & Goldich, S. S. (1961). New data for hisingerite and neotoctite. *The American Mineralogist*, *46*, 1412–1423.

Yen, A. S., Ming, D. W., Vaniman, D. T., Gellert, R., Blake, D. F., Morris, R. V., et al. (2017). Multiple stages of aqueous alteration along fractures in mudstone and sandstone strata in Gale Crater, Mars. *Earth and Planetary Science Letters*, *471*, 186–198. https://doi.org/10.1016/j.epsl.2017.04.033